

LDACS1 RANGING PERFORMANCE - AN ANALYSIS OF FLIGHT MEASUREMENT RESULTS

Dmitriy Shutin, Nicolas Schneckenburger, Michael Walter, Michael Schnell
German Aerospace Center (DLR), 82234 Wessling, Germany

Abstract

An L-band Digital Aeronautical Communication System type 1 (LDACS1) has been recently proposed to provide an Alternative Positioning, Navigation, and Timing (APNT) service for aeronautics during possible GNSS (Global Navigation Satellite System) outages. To validate the use of LDACS1 communication signals as ranging sources in realistic scenarios, a flight measurement campaign has been performed. This paper presents and discusses the ranging results obtained from the data collected in the measurement flight. Based on the analysis of the measured data, it can be concluded that LDACS1 signals offer an excellent ranging source, with ranging errors below 20m, which makes them suitable for implementing a future APNT service.

Introduction

Currently, aeronautical communications and navigation are undergoing a major renovation process to assist modernization of Air-Traffic Management (ATM) as developed under NextGen [1] and SESAR [2] in US and Europe, respectively.

An L-band Digital Aeronautical Communication System type 1 (LDACS1) [3] is currently one of the most actively developed novel aeronautical communication systems to provide a future air-traffic data link. It employs a broadband transmission using Orthogonal Frequency-Division Multiplexing (OFDM) and frequency division duplex (FDD) for forward and reverse channels. The LDACS1 channels are intended to be placed in spectral holes between neighboring Distance Measuring Equipment (DME) channels in L-band; the holes are formed due to the spectral shape of the DME pulses. Such an “in-lay” deployment strategy of the LDACS1 channels, on the one hand, does not require any new dedicated spectral resources; on the other hand, it ensures an uninterrupted use of legacy DME equipment for navigation.

In aeronautical navigation a transition is also taking place. In future, it is foreseen by ICAO to

make use of Global Navigation Satellite System (GNSS) technologies and corresponding augmentation systems (e.g., Satellite and Ground Based Augmentation Systems, Advanced Receiver Autonomous Integrity Monitoring, etc.), as primary means for navigation. Moreover, GNSS services are to be used not only for area navigation, but also for approach, take-off, and landing even under CAT III conditions.

Yet one of the major drawbacks of GNSS is a large separation between the navigational satellites and a receiver: the received signal strength of GNSS signals on the ground is very low. As a result, the received signal can be easily interfered with or jammed by terrestrial systems [4], [5]. To make sure that the navigation services are available even during possible GNSS outages or blockages, an alternative solution, commonly referred to as Alternative Positioning, Navigation, and Timing (APNT), is needed.

Essentially, a realization of an alternative navigational functionality requires an aircraft to be able to perform ranging to several known, typically ground-based¹ signal sources at known locations. Different ranging sources have been proposed and discussed by the community. One solution is to increase the density of Distance Measuring Equipment (DME) [6], [7] stations, which are currently used as primary radio-navigational aids. This approach has several disadvantages. Most importantly, it requires a costly extension of the DME infrastructure. Specifically, the DME stations are often located along air traffic corridors and, thus, their placement is not optimized for multilateration. Also, DME signal specifications, and thus ranging accuracy, have been defined with capabilities of now-outdated analog designs in mind; the DME system uses the L-band frequency spectrum very

¹ In principle, ranging can also be performed to other “non-navigational” satellites, provided their orbit can be computed. However, such ranging sources are often susceptible to the same kinds of interferences as GNSS services.

inefficiently. Moreover, the DME pulses are also known to cause interferences to Galileo E5a/E5b and GPS L5 signals [8]. Although “evolutionary” improvements of the DME are possible [7], the required extensions are comparable with the complete redesign of the DME infrastructure. Furthermore, such an extension might severely impact the sustainable use of the L-band for communications as foreseen within ICAO. Specifically, the L-band will be used more intensively by DME. This will make it difficult, or even impossible, to allocate sufficient spectrum resources for covering the growing demand for digital communications expected on a mid- and long-term as well as enhance the interferences to future GNSS services.

Another approach consists of integrating the navigation functionality into LDACS1 communication infrastructure [9]. Specifically, LDACS1 ground stations transmit continuously and synchronously in different frequency bands; each 500kHz-wide OFDM channel can be utilized as a ranging source [10]. In this way the navigational functionality is covered through the implementation of LDACS1 ground stations. Moreover, provided the LDACS1 can reliably cover the navigational function, an extension of the DME infrastructure for APNT is not necessary and even partial removal of DME ground stations might be possible. In this case, the L-band spectrum available for communications is increased and a sustainable use of the L-band for communications and navigation is assured.

In order to validate the LDACS1-based proposal for the APNT service, the German Aerospace Center has initiated a research project, termed LDACS-NAV. Its aim is to implement the core structure of the LDACS1 system for navigation and test its performance in a realistic scenario. Specifically, the goals of the campaign were to perform a flight measurement test with a core LDACS1 ground infrastructure and an airborne receiver [11]. The flight campaign was realized in November 2012. Within this paper we provide a short outline of the measurement campaign and discuss the ranging results obtained based on measured LDACS1 signals.

Description of the Measurement Setup

In this section we give a brief overview of the used measurement setup. For more information the reader is referred to [11], [12].

The future LDACS1-based navigation service would require a ranging to a minimum of four stations to estimate the aircraft position in 3D and a clock offset at the receiver². To this end the measurement setup consisted of four ground stations (GS) and a single receiver in a research aircraft Dassault Falcon 20, provided by the German Aerospace Center (see Figure 1).



Figure 1. Dassault Falcon 20E (D-CMET) employed in the measurement campaign.

The four ground stations were located in the area south west of the German Aerospace Center site in Oberpfaffenhofen (see Figure 2).



Figure 2. Ground Station locations (©OpenStreetMap).

The exact positions and frequencies are given in Table 1. Station A is set up at the airport in Oberpfaffenhofen, Station B is placed on an open area next to a detached house near Marktoberdorf, Station C is installed at a small airport for general aviation in Bad Woerishofen, and the station D is

² Unless other sensors, such as barometric or inertial sensors, are used.

located at the site of the german weather station Hohenpeissenberg.

Distance [km] from/ to	A	B	C	D
A - $f = 973.75$ MHz 48°5'8.91"N, 11°16'37.46"E	-	60	50	36
B - $f = 971.25$ MHz 47°45'5.53"N, 10°38'48.20"E	60	-	30	30
C - $f = 968.75$ MHz 48°0'58.99"N, 10°36'48.63"E	50	30	-	39
D - $f = 966.25$ MHz 47°50'4.57"N, 11°6'59.38"E	36	30	39	-

Table 1. GS positions and frequencies

Each GS was designed to transmit an LDACS1 signal with 10W transmit power. Channels are placed in a lower L-band between 965-975 MHz, as shown in Figure 3.

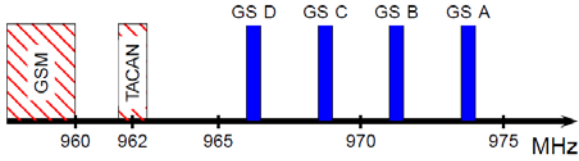


Figure 3. Frequencies of the stations and adjacent users.

Currently, there are no other users assigned to that band, with the closest possible interferers being a TACAN station at the military airport in Erding and a GSM band below 960 MHz. The hardware components of each GS included a Rb (Rubidium) atomic clock reference (with a single exception of station A that used a Cesium clock reference), a GPS time receiver for off-line station synchronization (see [12] for more details on station synchronization), an arbitrary waveform signal generator to generate bandpass versions of an LDACS1 signal, and a power amplifier with appropriate bandpass filters to reduce out-of-band emissions. The schematic setup of a GS is shown in Figure 4.

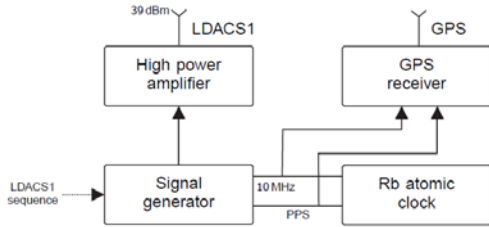


Figure 4. Setup of a ground station.

The Falcon aircraft has been equipped with the recording equipment (data grabber) that was used to store the sampled LDACS1 channels on a harddisk for further offline processing. The setup of the airborne station is shown in Figure 5.

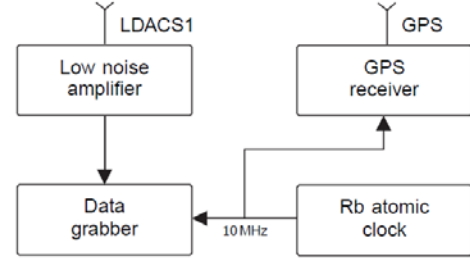


Figure 5. Setup of an airborne station.

Note that this setup also includes a GPS receiver that provides the ‘ground truth’ range and positioning information. The range estimates obtained based on the LDACS1 signals will then be compared to the GPS-based estimates.

The LDACS1 signal used in the experiments was designed following the LDACS1 forward link specifications [3]. The parameters of the signal are shortly summarized in the Table 2.

Parameter	Value
Bandwidth	500 kHz
Nominal transmit power	39 dBm
DFT size	64
Used subcarriers	50
Subcarrier spacing	≈ 9.7 kHz
Superframe (SF) length	240 ms
OFDM symbols in SF	2000
Sampling time	1.6 μ s
Total symbol duration	120 μ s
Windowing duration	12.8 μ s
Cyclic prefix duration	4.8 μ s

Table 2. LDACS1 signal transmission parameters.

A single transmission included 4 superframes followed by a 40ms pause. This resulted in 8000 OFDM symbols per second that were used for ranging. The OFDM symbols were randomly generated to reduce the peak to averaged power ratio.

The campaign was executed in November 2012. Before start and after landing, station A, mounted in a van, met the aircraft on the apron for clock synchronization. The pattern shown in Figure 6 was flown on three different altitudes, flight level 90

($\approx 3000\text{m}$), 310 ($\approx 8500\text{m}$), and 390 ($\approx 11500\text{m}$). Hereby, the aircraft flew a 'butterfly' pattern over the stations, using each station as turning point. This allows for an analysis of different real world geometric constellations. The entire flight took about 90 minutes.

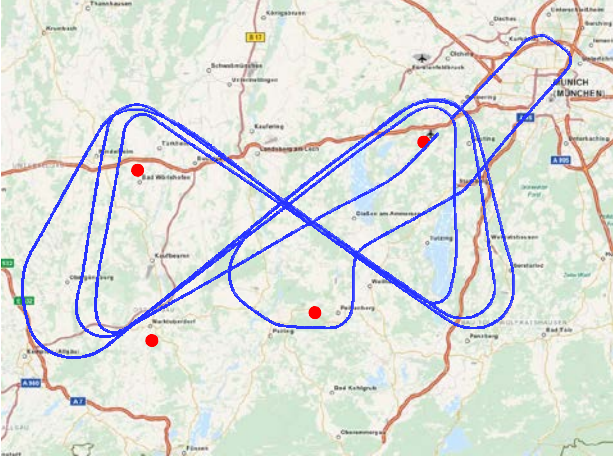


Figure 6. Route of the flight conducted on Nov. 13th, 2012 (© OpenStreetMap).

Processing of the measurement data

In what follows we present a detailed evaluation of the results from the flight measurement campaign. Focus is put on the ranging performance, since the quality of the range estimates is crucial for the achievable navigation performance in terms of accuracy, precision, and integrity. To this end we consider ranging to the Station A located in Oberpfaffenhofen.

Consider now a simplified model for the estimated range between the aircraft and station A:

$$\mathbf{r}_{est} = \mathbf{r}_{true} + \mathbf{c}\tau_{HW} + \mathbf{c}(t_{GS} - t_{AIR}) + \boldsymbol{\varepsilon}, \quad (1)$$

where \mathbf{r}_{est} is a measured range obtained with classical range estimation schemes, c is a speed of light, \mathbf{r}_{true} is an actual (unknown) range between the stations, τ_{HW} is a delay due to the hardware components in the transmitter and receiver, and $(t_{GS} - t_{AIR})$ is clock offset between GS and an airborne system clocks³. The perturbation $\boldsymbol{\varepsilon}$ accounts for all other (not necessarily random) errors, such as

³ Note that the clock offset $(t_{GS} - t_{AIR})$ is relevant only for the computation of the true range between the GS and an airborne receiver. For positioning, the clock offset is assumed unknown and is estimated through solving the navigational equation.

multipath propagation, tropospheric delays, and white random noise.

Some of these factors can be effectively controlled within the used experimental setup.

Calibration of the Station A

The delays caused by the transmitter and receiver hardware of the measurement system can be compensated through an accurate calibration of the devices. As outlined in [11], the calibration of the Station A aims at estimating the transfer function of the whole transmission path between the corresponding transmitter and receiver when the clocks of both stations are manually phase- and frequency- aligned.

The baseband version $C(e^{j\theta})$ of the calibration data can be represented as⁴

$$C(e^{j\theta}) = R(e^{j\theta})T(e^{j\theta})S(e^{j\theta}) \quad (2)$$

where $S(e^{j\theta})$ a transmitted LDACS1 signal, and $T(e^{j\theta})$ and $R(e^{j\theta})$ are the baseband frequency responses of the transmitter and receiver hardware, respectively. Note that since calibration is performed through a cable, the calibration data has a very high signal-to-noise ratio. Let us mention that the calibration through the cable does not account for responses of the transmitting and receiving antennas; since the antenna delays were relatively small in comparison to the other factors, they were ignored in the further processing. During the actual measurement the signal between the transmitter and receiver will undergo a linear transformation by the channel with the baseband frequency response $H(e^{j\theta})$ that accounts for all other signal delays. Thus, a received signal $Y(e^{j\theta})$ can then be represented as

$$\begin{aligned} Y(e^{j\theta}) &= R(e^{j\theta})H(e^{j\theta})T(e^{j\theta})S(e^{j\theta}) + E(e^{j\theta}) \\ &= C(e^{j\theta})H(e^{j\theta}) + E(e^{j\theta}) \end{aligned} \quad (3)$$

where $E(e^{j\theta})$ is additive measurement noise. During the estimation, the measured signal is correlated with a normalized version of the calibration signal $\tilde{C}(e^{j\theta}) = C(e^{j\theta})/|C(e^{j\theta})|^2$. The correlation with the calibration data effectively cancels the influence of the delay τ_{HW} on the range estimation.

⁴ Here we assume the linearity of the measurement equipment.

Note also that the normalization of the calibration data is well defined, since $C(e^{j\theta})$ is not zero at the frequencies of interest. The estimated amplitude and phase responses for the calibration data $C(e^{j\theta})$ are summarized in Figure 7 and Figure 8. Note, that despite the fact that the phase response of $C(e^{j\theta})$ does not allow computing the absolute delay of the measurement equipment, the variations of the resulting group delay around the mean can be computed. These are summarized in Figure 9. As it can be seen, the corresponding variations do not exceed 0.6m, with standard deviation being equal to only 17 cm.

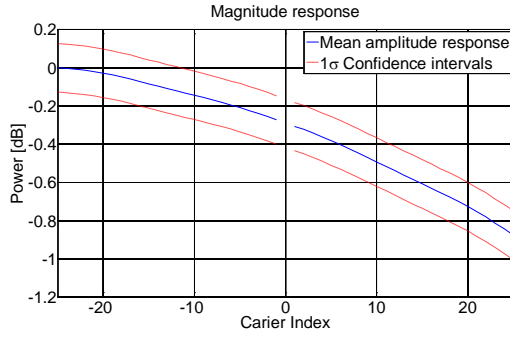


Figure 7. Amplitude response of $C(e^{j\theta})$ normalized to the maximum averaged magnitude.

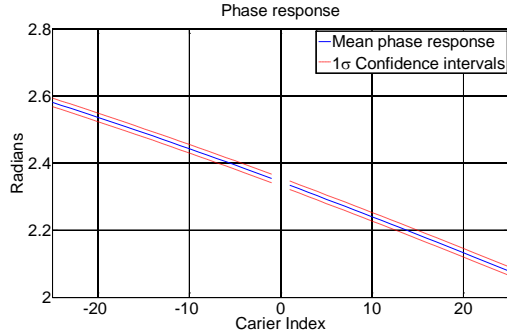


Figure 8. Phase response of $C(e^{j\theta})$.

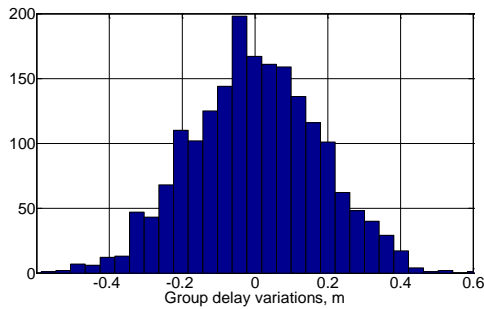


Figure 9. Group delay variations of the measurement setup.

Computing the clock offset between the Station A and an airborne receiver clock.

Another factor that can be controlled within the measurement setup is a clock offset between the Station A and a receiver clock. As it has been mentioned, the Station A used highly stable cesium clock that was running synchronously with the GPS time. During the calibration, the receiver clock was manually aligned with Cesium clock, yet during the measurements it drifted away. To capture the drift, the data grabber (receiver) time-stamped the measured GPS time using receiver clock. Over the course of measurements, the drift between the receiver clock and GPS time grew larger. The smoothed version of it has been used as an estimate of the clock offset ($t_{GS} - t_{AIR}$). The measured and estimated clock drift are shown in Figure 10.

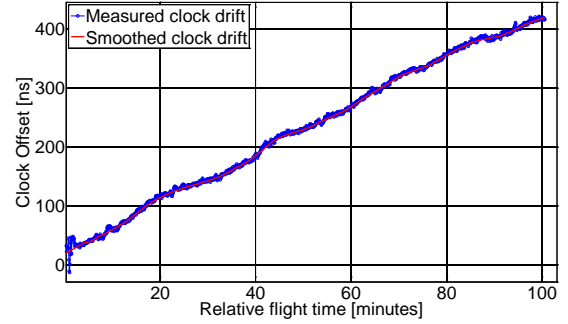


Figure 10. Estimated clock drift between the Station A and airborne receiver.

Observe that during the measurement time the airborne clock drifted almost 400ns. Yet, the drift is almost linear and well predictable.

Range estimation results

Assuming that the propagation channel between the transmitter and receiver consists purely of single propagation path (line of sight), the range estimation can be solved by correlating the received signal $Y(e^{j\theta})$ with calibration data $\tilde{C}(e^{j\theta})$

$$\begin{aligned}\tilde{C}(e^{j\theta})Y(e^{j\theta}) &= \tilde{C}(e^{j\theta})C(e^{j\theta})H(e^{j\theta}) \\ &\quad + \tilde{C}(e^{j\theta})E(e^{j\theta}) \\ &= H(e^{j\theta}) + \tilde{E}(e^{j\theta}),\end{aligned}\quad (4)$$

followed by the analysis of the phase of response of the (4) or maximum search (in time domain).

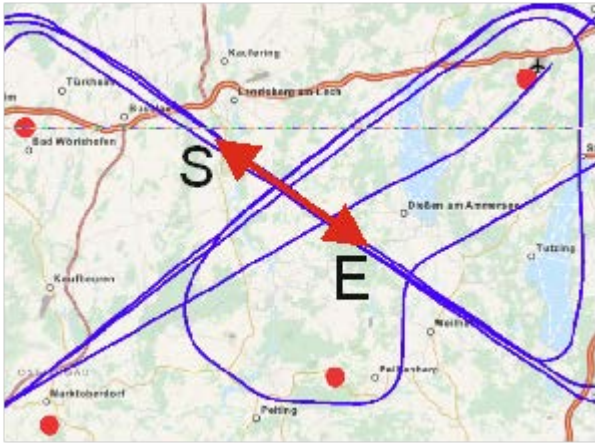
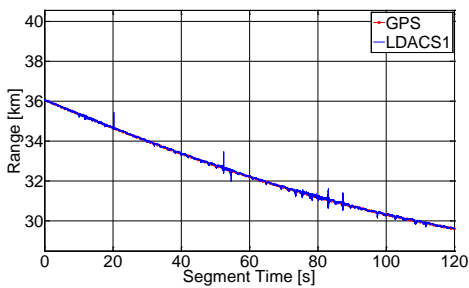


Figure 11. Analyzed measurement segment.

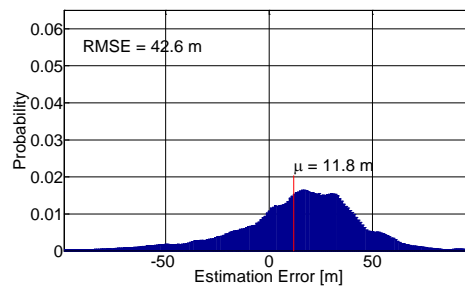
In our work we used the latter method, as it was found to be less sensitive to interference.

In what follows we present the estimation results obtained with this method for different segments of the flight. For this purpose we select a 2-minute segment between the stations, as shown in Figure 11 between the points S and E. Three different altitudes for the segment were considered: FL90, FL310 and FL390. The corresponding estimation results are summarized in Figure 12, where the estimated ranges as well as empirical distribution errors are plotted.

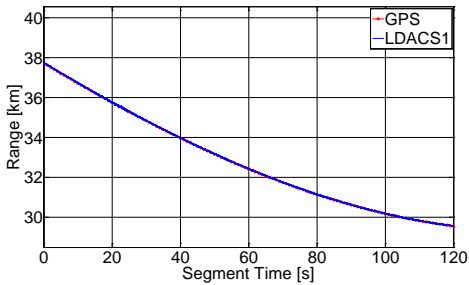
Note that for lower altitudes the ranges estimation is worse than for higher altitudes. The estimation bias also reduces for higher altitudes. Our explanation for this behavior is that several major factors can affect



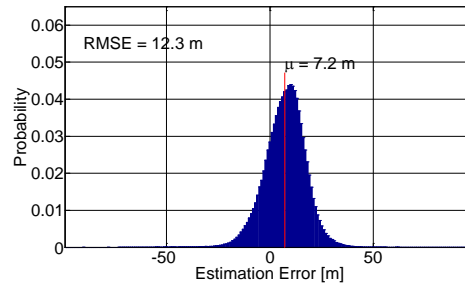
a)



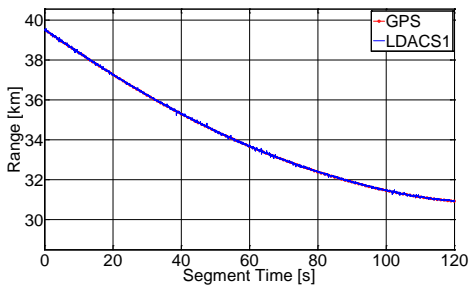
d)



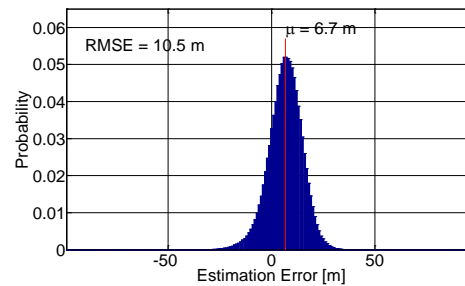
b)



e)



c)



f)

Figure 12. Estimated ranges and range errors computed for the selected segment of the flight trajectory for (a,d) FL90, (b,e) FL310, and (c,d) FL390. Figures (a),(b) and (c) show the estimated range versus the corresponding range computed based on the GPS coordinates of the airplane. Figures (d),(e) and (f) show the empirical distributions range error distributions.

the performance of the estimator at lower elevation angles: (i) the tropospheric effects might lead to higher estimation bias, (ii) the relative position difference of the receiving GPS antenna, which was on the top of the fuselage, and the LDACS1 receiving antenna, which was located on the bottom. Since the antennas were not collocated, the true range estimated based on GPS data depends on the exact role, pitch and yaw of the airplane. Finally, (iii) the multipath effects, which will consider later in the text, significantly impact the increased variability of the range estimates; these were observed to be severe (in some extreme case) at lower altitudes, especially during banking turns.

In the next plot we show the range error distribution for the whole measurement flight.

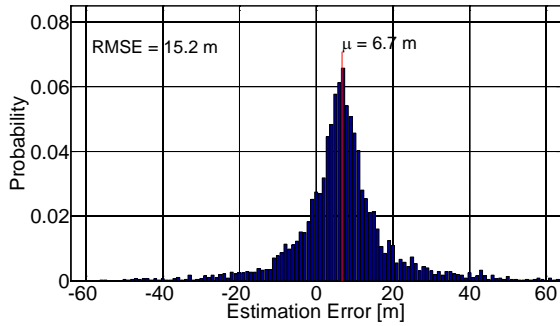


Figure 13. RMSE of range estimation for the whole measurement flight.

The results in Figure 13 were obtained by performing a linear fit to the 8000 range estimates over a 1 second interval and comparing those to the GPS-based range estimates. The statistic excludes a single non-LOS case observed at FL90, which resulted in range error of more than 2000 meters (see also the following section). Let us note that for the whole flight the RMSE of range estimation is only 15.2 meters, with 99 percentile corresponding to only 50 meters.

Impact of the DME on the ranging performance

The spectral proximity of the LDACS1 signals to DME makes them in general susceptible to the interference from the latter navigational system. The DME interference is a part of the perturbation ϵ in the model (1). It can also be seen from the Figure 12a that the estimated range exhibits impulse-like errors at multiple time instances. These errors are caused by

co-site interference from the onboard DME transmitter. The frequency and time domain waveforms of the LDACS1 symbol perturbed by the DME pulse are shown in Figure 14.

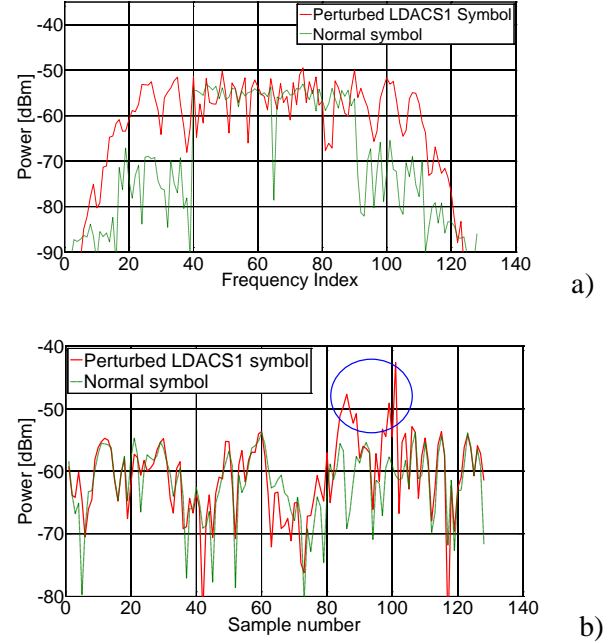


Figure 14. a) Power spectrum and b) time domain waveforms of the LDACS1 symbol perturbed by a co-site DME interference. The shown symbols were oversampled by a factor of 2.

The shown interference has been measured at a distance of 51km from station A and an altitude of 9,560 feet. Observe that the co-site interference affects the whole symbol bandwidth. In fact, this interference is seen by the receiver as a wideband noise from the airborne DME transponder; it thus cannot be effectively filtered out. Instead, the whole OFDM symbol should be discarded. Provided the DME pulse can be detected [13], the corresponding affected symbol can be simply discarded and not used for ranging without reducing the system performance. This is simply due to the fact that currently the system produced 8000 range measurement per second; thus, discarding a few symbols should not have a significant impact on the system performance.

Impact of the multipath propagation on the ranging performance

Another factor that effects the perturbation ϵ in (1) is the multipath propagation. The analysis of the

measurement data has also revealed a significant impact of the multipath propagation on the ranging performance, especially at low altitudes. The transmitting antenna of the station A has been placed at the airport Oberpfaffenhofen. Due to a specific placement of the antenna dictated by the regulations of the airport, the surrounding airport infrastructure created a multipath propagation environment that had a measurable impact on the performance of the range estimator.

In order to address the multipath problem, we consider a state-of-the-art super-resolution multipath estimation algorithm. The algorithm is based on fast variational sparse Bayesian parameter estimation scheme [14] and a classical Kalman filter [15], used for tracking individual multipath components. The former algorithm allows for incremental estimation of the parameters of multipath components, which are the delay and Doppler frequency of each propagation path, as well as automatic estimation of number of components detectable in measurement data. Using Kalman filter individual propagation paths can then be tracked over time. In Figure 15 we show sample ranging results obtained with this tracking algorithm, which we term sparse adaptive multipath estimation (SAME) algorithm. The results are compared to a simple correlator, which is optimal under pure line-of-sight (LOS) assumption.

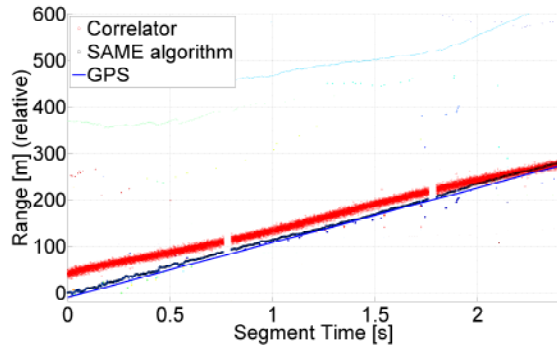


Figure 15. Multipath mitigation with Superresolution parameter estimation.

It can be observed that the correlator output is affected by the presence of multipath components that are roughly 300-400m away from the LOS component. The resulting RMSE in this case is 30.04m. In contrast, the SAME algorithm follows the GPS range quite closely, mitigating the multipath interference and leading to the range RMSE of

6.76m. The next figure demonstrates even more severe multipath interference, which is nonetheless much easier to detect. In Figure 16 we show a non-line-of-sight (NLOS) case, where the main path has been attenuated by the airplane frame during a banking turn.

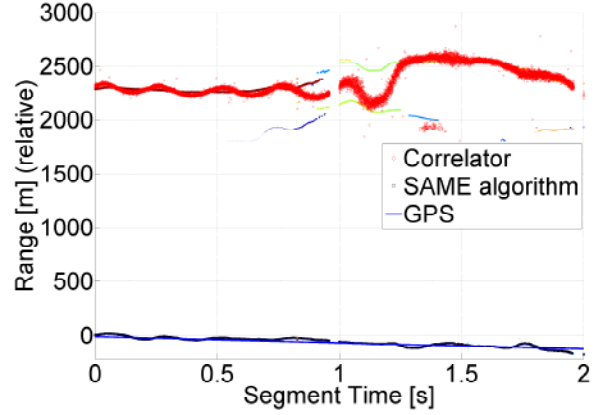


Figure 16. NLOS scenario at low flight levels during banking turns.

Such behavior has been observed in a single case at the lowest flight level. Note that here the main peak of the correlation function detects a multipath reflection that is almost 2000m away from the LOS path. The SAME algorithm, due to its tracking ability, allows for a removal of the multipath interference, keeping track of the LOS path even in the LOS-obstructed cases. The reduction of RMSE in this case is from 2430.64 meters (for the correlator), to 18.53 meters, for the SAME algorithm.

Summary and conclusions

In this paper we give a short overview of the ranging results from the flight measurement campaign aimed at validation and test of the LDACS1-based proposal for the APNT service. The flight measurement campaign, initiated by the German Aerospace Center, was implemented in November 2012. The estimated ranging performance indicates that RMSE errors far below 50 meters are achievable. This indicates a suitability of LDACS1-based navigation as a future APNT ranging source. However, as a ground-based system, LDACS1 system is affected more strongly by multipath propagation if the transmitting antennas are placed unfavorably. Thus special care must be taken when placing the transmit antennas in order to avoid

excessive multipath interference for any future ground-based APNT service.

References

- [1] NextGEN, “Federal Aviation Administration.” [Online]. Available: <http://www.faa.gov/nextgen/>.
- [2] “SESAR Joint Undertaking.” [Online]. Available: <http://www.sesarju.eu/>.
- [3] EUROCONTROL, “The LDACS1 Prototype Specifications (D3 Deliverable),” BRUSSELS, 2009.
- [4] A. H. Rutkin, “‘Spoofers’ Use Fake GPS Signals to Knock a Yacht Off Course,” *MIT Technology review*, 14-Aug-2013.
- [5] GPS World, “Massive GPS Jamming Attack by North Korea,” *GPS World*, 2012.
- [6] M. Kayton and W. R. Fried, Eds., *Avionics Navigation Systems*. John Wiley & Sons, Inc., 1969.
- [7] W. Pelgrum, “eDME architecture development and flight-test evaluation,” in *IEEE/AIAA 31st Digital Avionics Systems Conference (DASC)*, 2012.
- [8] G. X. Gao, “DME/TACAN Interference and its Mitigation in L5/E5 Bands,” *ION Institute of Navigation Global Navigation Satellite ...*, 2007.
- [9] M. Schnell, U. Epple, and F. Hoffmann, “Using the Future L-band Communication System For Navigation,” in *Integrated Communications Navigation and Surveillance Conference (ICNS)*, 2011.
- [10] N. Schneckenburger, D. Shutin, and M. Schnell, “Precise aeronautical ground based navigation using LDACS1,” in *Integrated Communications Navigation and Surveillance Conference (ICNS)*, 2012, pp. B1–1, B1–10.
- [11] D. Shutin, N. Schneckenburger, and M. Schnell, “LDACS1 for APNT — Planning and realization of a flight measurement campaign,” in *IEEE/AIAA 31st Digital Avionics Systems Conference (DASC)*, 2012, pp. 1–22.
- [12] N. Schneckenburger, B. P. B. Elwischger, B. Belabbas, D. Shutin, M.-S. Ciciu, M. Suess, M. Schnell, J. Furthner, and M. Meurer, “LDACS1 Navigation Performance Assessment By Flight Trials,” in *The European Navigation Conference (ENC)*, 2013.
- [13] U. Epple, D. Shutin, and M. Schnell, “Mitigation of Impulsive Frequency-Selective Interference in OFDM Based Systems,” *IEEE Wireless Communications Letters*, vol. 1, no. 5, pp. 484 – 487, 2012.
- [14] D. Shutin, W. Wang, and T. Jost, “Incremental Sparse Bayesian Learning for Parameter Estimation of Superimposed Signals,” in *10th International Conference on Sampling Theory and Applications*, 2013.
- [15] S. Kay, *Fundamentals of Statistical Signal Processing, Volume I: Estimation Theory (v. 1)*. Prentice Hall, 1993, p. 625.

Email Addresses

Dmitriy.Shutin@DLR.de

Nicolas.Schneckenburger@DLR.de

Michael.Walter@DLR.de

Michael.Schnell@DLR.de

*32nd Digital Avionics Systems Conference
October 6-10, 2013*